Finite-Temperature Properties of Ba(Zr, Ti)O₃ Relaxors from First Principles

A. R. Akbarzadeh,[1] S. Prosandeev,[2,3] Eric J. Walter,[4] A. Al-Barakaty,[5] and L. Bellaiche[2]

[1]*Wiess School of Natural Sciences, Rice University, 6100 Main Street, MS-103, Houston, Texas 77005, USA*
[2]*Physics Department and Institute for Nanoscience and Engineering, University of Arkansas, Fayetteville, Arkansas 72701, USA*
[3]*Physics Department and Institute of Physics, South Federal University, 344090 Rostov on Don, Russia*
[4]*Department of Physics, College of William and Mary, Williamsburg, Virginia 23187, USA*
[5]*Physics Department, Teacher College, Umm Al-Qura University, Makkah, Saudi Arabia*
(Received 8 April 2012; published 20 June 2012)

A first-principles-based technique is developed to investigate the properties of Ba(Zr, Ti)O₃ relaxor ferroelectrics as a function of temperature. The use of this scheme provides answers to important, unresolved and/or controversial questions such as the following. What do the different critical temperatures usually found in relaxors correspond to? Do polar nanoregions really exist in relaxors? If yes, do they only form inside chemically ordered regions? Is it necessary that antiferroelectricity develop in order for the relaxor behavior to occur? Are random fields and random strains really the mechanisms responsible for relaxor behavior? If not, what are these mechanisms? These *ab initio* based calculations also lead to deep microscopic insight into relaxors.

Relaxor ferroelectrics are characterized by some striking anomalous properties (see, e.g., Refs. [1–21] and references therein). For instance, they adopt a peak in their ac dielectric response versus temperature function while they remain macroscopically paraelectric and cubic down to the lowest temperatures [1]. Furthermore, this dielectric response deviates from the "traditional" Curie-Weiss law [22] for temperatures lower than the so-called Burns temperature [2]. Other examples of anomalous properties include the plateau observed in their static dc dielectric response at low temperatures [23,24], and the unusual temperature behavior [16] of the Edwards-Anderson parameter [25]. Determining the origin of these intriguing effects has been a challenge to scientists since the discovery of ferroelectric relaxors.

The goal of this Letter is to report *ab initio* based calculations that not only reproduce all the aforementioned intriguing features but also offer deep microscopic insight into relaxors.

Practically, we decided to focus on a specific relaxor, namely disordered Ba(Zr₀.₅Ti₀.₅)O₃ (BZT) solid solutions. (BZT is also fascinating because its parent compounds are rather different: BaZrO₃ is paraelectric while BaTiO₃ is a typical ferroelectric.) Here, we develop and use a first-principles-based effective Hamiltonian approach for which a detailed description is given in the supplemental material [26–39]. The total energy of this effective Hamiltonian is used in Monte Carlo (MC) simulations to compute finite-temperature properties of BZT alloys. We use $12 \times 12 \times 12$ (8640 atoms) or $16 \times 16 \times 16$ (20 480 atoms) supercells in which the σ_j variables are randomly placed and kept fixed during the MC simulations, in order to mimic disordered BZT solid solutions. These two supercells provide similar results, which attest to the convergency of the simulations. The temperature T is decreased in small steps from high temperature, and up to 10^6 MC sweeps are used to get converged statistical properties.

Here, the $\mathbf{u}_i$ local soft-mode vectors in each five-atom cell i ($\mathbf{u}_i$ is directly proportional to the local electric dipole moment centered in cell i) and the homogeneous strain tensor η_H arising from the MC simulations indicate that Ba(Zr₀.₅Ti₀.₅)O₃ bulk remains macroscopically *cubic and nonpolar* for *any* temperature down to the lowest one investigated here (which is 5 K), which is consistent with measurements [40]. We also computed the dielectric susceptibility, at different temperatures by progressively cooling down the system, from our MC simulations via two different approaches: (i) a "direct" method for which the resulting dielectric susceptibility is denoted as χ^{direct} and is calculated as the change in polarization with respect to an applied electric field (with this field practically being oriented along the [111] pseudocubic direction and having a magnitude of 10^7 V/m); and (ii) the "correlation-function" approaches of Refs. [41,42] for which the resulting dielectric susceptibility is referred to as χ^{CF} and is provided by the fluctuation-dissipation theorem via $\chi^{\text{CF}}_{\alpha\beta} = \frac{(NZ^*)^2}{V\epsilon_o k_B T}[\langle u_\alpha u_\beta \rangle - \langle u_\alpha \rangle \langle u_\beta \rangle]$, where $\langle u_\alpha u_\beta \rangle$ denotes the statistical average of the product between the α and β components of the supercell average of the local mode vectors, and where $\langle u_\alpha \rangle$ (respectively, $\langle u_\beta \rangle$) is the statistical average of the α (respectively, β) component of the supercell average of the local mode vectors. N is the number of sites in the supercell while V is its volume. k_B is Boltzmann's constant, and ϵ_o is the permittivity of the vacuum. Strikingly, while previous work (see, e.g., Ref. [42]) found that these two different methods provide nearly identical dielectric susceptibilities in typical ferroelectrics, Fig. 1(a)
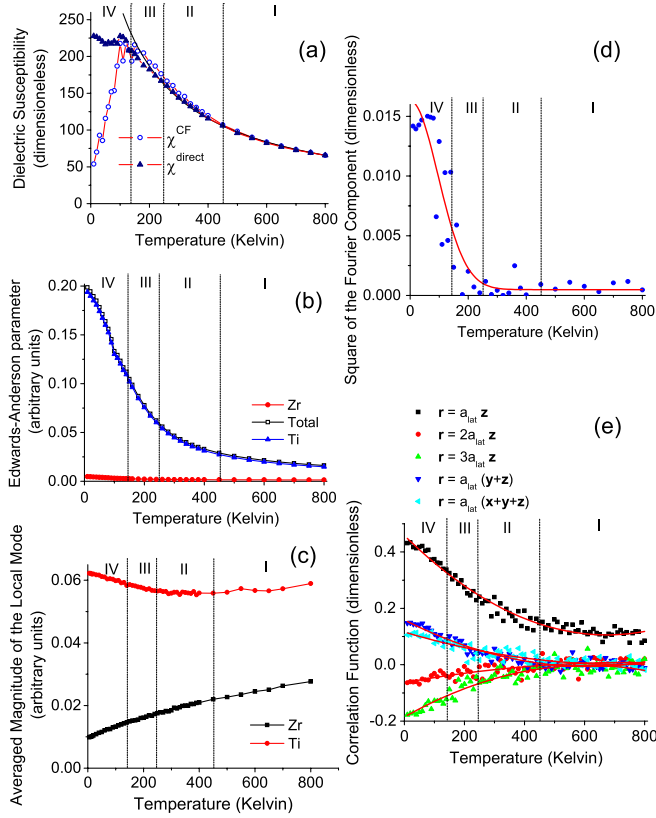
FIG. 1 (color online). Temperature dependence of some properties in disordered Ba(Zr$_{0.5}$Ti$_{0.5}$)O$_3$ solid solutions. Panel (a) shows the average between the three diagonal elements of the dielectric susceptibility, as computed from a direct approach (χ^{direct}, triangles) and from the fluctuation-dissipation theorem (χ^{CF}, dots). Panel (b) displays the total Edwards-Anderson parameter, as well as its contributions from cells centered on Ti and Zr ions. Panel (c) reveals the magnitude of the local modes centered on Ti and Zr ions. Panel (d) represents the square of the Fourier transform of the local modes' configurations at $\mathbf{k}_{\max}$. Panel (e) provides the $\theta(\mathbf{r})$ correlation between Ti dipoles for $\mathbf{r} = a_{\text{lat}}\mathbf{z}$ (first nearest neighbor), $a_{\text{lat}}(\mathbf{y} + \mathbf{z})$ (second nearest neighbor), $a_{\text{lat}}(\mathbf{x} + \mathbf{y} + \mathbf{z})$ (third nearest neighbor), $2a_{\text{lat}}\mathbf{z}$, and $3a_{\text{lat}}\mathbf{z}$. The solid line in Panel (a) represents the dielectric susceptibility arising from the fit of χ^{CF} (between 500 and 800 K) by the Curie-Weiss law [22].

reveals that it is not the case for disordered BZT: χ^{CF} exhibits a peak around $T_f \simeq 130$ K, while χ^{direct} increases when decreasing the temperature down to T_f and then saturates to a plateau for lower temperature. Both the temperature behavior of χ^{CF} and the temperature at which χ^{CF} is maximum are fully consistent with the dielectric experiments of Ref. [40] in Ba(Zr$_x$Ti$_{1-x}$)O$_3$ *relaxors* under ac electric fields having frequencies ranging between 100 Hz and 100 kHz. Moreover, the depicted behavior of χ^{direct} is exactly the one expected for the perfectly *static* dielectric response of relaxors [23,24], which allows us to identify T_f as the so-called freezing temperature [7–10] (a freezing temperature ranging between 100 and 140 K has

been reported for BZT systems [43], in good agreement with our value of $\simeq 130$ K). Our χ^{direct} thus provides the static (dc) dielectric response while our simulated χ^{CF} corresponds to observed low-frequency dielectric responses of BZT relaxors—which is reminiscent of the fact that the susceptibility given by the fluctuation-dissipation theorem is nearly the ac susceptibility in the Edwards-Anderson model of spin glasses [44].

It is also important to recall that, while χ^{CF} possesses a peak at T_f, our MC simulations indicate that Ba(Zr$_{0.5}$Ti$_{0.5}$)O$_3$ bulk remains macroscopically *cubic and nonpolar* for *any* temperature—which is consistent with what is expected for relaxors [1]. Moreover, the temperature behaviors of χ^{CF} and χ^{direct} allow the introduction of four different regions: namely, (1) Region I that concerns temperatures, T, above $T_b \simeq 450$ K and for which χ^{CF} and χ^{direct} can be nicely fitted by the Curie-Weiss formula [22]; i.e., they are both directly proportional to $1/|T - T_0|$ (where T_0 is practically found here to be very close to -120 K); (2) Region II that extends between $T^* \simeq 240$ K and T_b for which χ^{CF} increases as the temperature decreases but no longer follows the Curie-Weiss law, unlike χ^{direct}; (3) Region III that is located in between T_f and T^* for which neither χ^{CF} nor χ^{direct} obey the Curie-Weiss law; and (4) Region IV that occurs for temperatures lower than T_f, and for which χ^{CF} decreases as T is reduced while χ^{direct} is nearly constant there. T_b can be assigned to be the Burns temperature [2] while T^* can be thought of as being the novel critical temperature recently found in relaxors [11,12]. The facts that χ^{CF} follows the Curie-Weiss law only for temperatures above the Burns temperature and that this Burns temperature is of the order of 450 K have both been observed in Ba(Zr$_{0.5}$Ti$_{0.5}$)O$_3$ [40]. Similarly, a *negative* T_0 Curie temperature has also been experimentally extracted in BZT samples [40].

Figure 1(b) reports the temperature evolution of the so-called Edwards-Anderson parameter [25], q_{EA}, that is calculated as $q_{\text{EA}} = \langle\langle Z^* \mathbf{u}_i \rangle_t^2 \rangle_i$, where the inner averaging is made over the t Monte Carlo sweeps while the outer averaging is made over the i lattice sites. The behavior of the simulated q_{EA} of BZT bulk versus temperature bears some striking resemblance with those predicted by the spherical random bond–random field model and measured from nuclear magnetic resonance for the PbMg$_{1/3}$Nb$_{2/3}$O$_3$ relaxor [16]. For instance, (1) it is small and increases nearly linearly with decreasing temperature at high temperatures (in Region I); (2) it is large and also increases linearly with decreasing temperature at low temperatures (in Region IV); and (3) the q_{EA}-versus-T function is curved upward in between (in Regions II and III). Figure 1(b) also reveals that the temperature behavior and values of the overall Edward-Anderson parameter (for any temperature) almost entirely originate from the electric dipoles centered on Ti ions. Consequently, the contribution of the dipoles belonging to BaZrO$_3$ unit cells to the total

Edwards-Anderson parameter nearly vanishes. Other dramatic differences between local properties associated with Zr versus Ti atoms are revealed in Fig. 1(c), which shows that not only is the average magnitude of the local dipoles centered on Zr ions much smaller than those centered on Ti ions, but its temperature behavior is also strikingly different: the dipoles belonging to $BaZrO_3$ unit cells continuously shrink on average as the temperature is reduced, while the dipoles located inside $BaTiO_3$ cells suddenly become enlarged with decreasing temperature below T^*. Electric diffraction measurements [39] and a model emphasizing the importance of the $BaTiO_3$ soft mode on the relaxor behavior of BZT [45] are also consistent with our prediction that the Ti sites carry much larger dipoles than the Zr sites. Moreover, the results from Fig. 1(c) imply that, at the lowest temperatures, the Ti atoms displace on average about 0.16 Å, while the Zr atoms move by 0.03 Å from their cubic, equilibrium positions. Such numbers are in remarkable agreement with the values of 0.17 and 0.03 Å, respectively, obtained by the first-principles calculations of Ref. [46] for a BZT supercell containing 135 atoms [47].

Let us now focus on Fig. 2, which displays dipolar snapshots within a given (y, z) plane at different temperatures, in order to gain a microscopic understanding of relaxors. Figure 2(a) reveals that Region I consists of randomly oriented dipoles that are centered on Ti ions and that are surrounded by much smaller dipoles located inside $BaZrO_3$ cells. As indicated in Fig. 2(b), some of these Ti sites act as nuclei to the formation of small clusters inside which the dipoles begin to be parallel to each other in Region II. We numerically found that the polarization of these small clusters in Region II does not automatically lie along a $\langle 111 \rangle$ direction. For instance, the average direction of the local modes inside the bottom cluster of Fig. 2(b) is
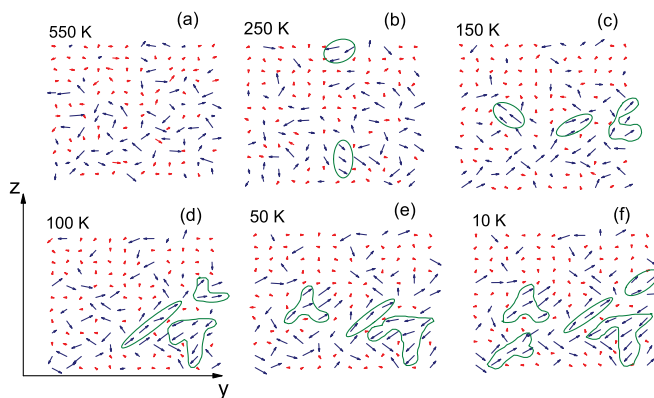
along an orthorhombic-like direction, namely it is close to $[01\bar{1}]$. Interestingly, some of these clusters do not even possess a polarization that is parallel to a high symmetry direction in Region II, such as the top cluster of Fig. 2(b) for which the vector resulting from the average of the local modes is equal to $(-0.012, -0.052, -0.021)$ in the (x, y, z) basis—that is, a triclinic direction. It is interesting to realize that thermal strain measurements [40] strongly suggest that polar nanoclusters can exist in BZT up to $\simeq 440$ K, which is consistent with our finding of small polar clusters in Region II (that extend up to $T_b \simeq 450$ K).

As the system enters Region III, two novel features occur that can be inferred from Fig. 2(c). First, more (small) polar clusters form as the temperature is decreased, which makes the average magnitude of the Ti dipoles increase [see Fig. 1(c)]. Second, some of these clusters now possess a polarization close to the $\langle 111 \rangle$ direction, such as the left and right clusters displayed in Fig. 2(c) for which the average local modes are equal to $(0.043, -0.048, 0.043)$ and $(0.034, 0.037, 0.045)$, respectively. Note that, while the clusters are always formed at Ti sites, they do not necessarily stay at the same sites for different temperatures, or even for different MC sweeps at the same temperature, in Regions II and III. In that sense, they can be thought of as being of dynamical nature rather than being static.

Below T_f, some of these clusters have considerably grown in size, like the one located at the bottom right corners in Figs. 2(d)–2(f). Novel clusters can still form when decreasing the temperature in Region IV, such as the one near the bottom left corner of Fig. 2(f) at 10 K. On the other hand, other clusters are frozen in the sense that they are always located at the same region of space and have a polarization that lies along the same direction, independently of the temperature and MC sweep in Region IV (see the central and bottom right clusters in Fig. 2(d)–2(f). While the different clusters possess different numbers of Ti sites and have different overall shapes, they share a common feature in Region IV: they all have a polarization close to one of the eight equivalent $\langle 111 \rangle$ directions, consistent with the experimental finding that Raman spectra indicate a rhombohedral structure for the polar regions at liquid nitrogen temperature in BZT relaxors [48]. As the temperature is reduced in Region IV, the matrix possesses Zr-centered dipoles that are significantly shrinking in magnitude. This matrix in Regions II, III, and IV also possesses individual Ti dipoles that are oriented along many different directions, as in Region I.

To gain further insight into the relaxor behavior, let us denote as $\mathbf{k}_{max}$ the vector of the first Brillouin zone possessing the largest magnitude of the Fourier transform of the local dipoles configuration [49]. $\mathbf{k}_{max}$ is numerically found to be slightly dependent on the choice of the supercell used, but is always a nonhighly symmetric vector that is close to neither the center nor the boundary of the cubic first Brillouin zone. For instance, in case of a $12 \times 12 \times 12$

FIG. 2 (color online). Snapshots of the dipolar configurations in a given (y, z) plane for different temperatures. Panels (a), (b), (c), (d), (e), and (f) correspond to temperatures of 550 K (Region I), 250 K (Region II), 150 K (Region III), 100 K (Region IV), 50 K (Region IV) and 10 K (Region IV), respectively. Blue colors and red colors indicate that the corresponding local modes are centered on Ti and Zr ions, respectively.

supercell, $\mathbf{k}_{\max} = \frac{2\pi}{6a_{\text{lat}}}(-\mathbf{y} + \mathbf{z})$, where a_{lat} is the lattice constant of the five-atom primitive cell and where $\mathbf{y}$ and $\mathbf{z}$ are unit vectors along the y- and z-axes, respectively. Figure 1(d) shows the temperature evolution of the square of the Fourier transform of the local dipoles configuration at $\mathbf{k}_{\max}$. One can clearly see that, in Regions I and II, this quantity is nearly zero. On the other hand, it increases when the temperature decreases below T^* while still remaining fairly small (around 1.5% of the total spectra gathering the Fourier transforms at all possible k-points, at 5 K). We interpret such latter results as indicative that the different nanopolar regions slightly interact in Regions III and IV in an antiferroelectriclike (or incommensurate [50] or dipolar-wave-like) fashion. Interestingly, antiferroelectricity has been previously reported in some relaxor systems [14,15].

Let us now compute the correlation between Ti dipoles (we decided to focus on Ti-Ti dipolar correlations because Fig. 2 revealed that the polar clusters only contain Ti sites and because Fig. 1(b) shows that the overall Edwards-Anderson parameter mainly only originates from Ti dipoles). This correlation is practically defined by $\theta(\mathbf{r}) = \frac{1}{N_{Ti}}\sum_i \frac{\mathbf{u}_i \cdot \mathbf{u}_{i+r}}{|\mathbf{u}_i||\mathbf{u}_{i+r}|}$, where the index i runs over all the N_{Ti} Ti sites of the system and where $\mathbf{u}_i$ and $\mathbf{u}_{i+r}$ are the local modes in cell i and in the cell centered on the Ti atom (if any) distant from $\mathbf{r}$ from the cell i, respectively [51]. A value of 1 (respectively, -1) for $\theta(\mathbf{r})$ for a given $\mathbf{r}$ would indicate that Ti dipoles and their neighboring Ti dipoles distant from $\mathbf{r}$ are aligned along the same (respectively, opposite) direction. Figure 1(e) shows the value of $\theta(\mathbf{r})$ for various representative $\mathbf{r}$ vectors, as a function of temperature. One can see that, in Region I and on average, the Ti dipoles are only (and slightly) correlated with the Ti dipoles centered at their first nearest neighbor cells. Such a correlation further increases in strength when the polar nanoclusters form and become greater in size and in polarization, as the temperature is reduced in Regions II, III, and IV. Second- and third-nearest neighbors also begin to be more correlated on average as the temperature decreases in Regions III and IV. Interestingly, a significant *anticorrelation* (see the negative sign of the correlation) between Ti dipoles that are distant by three lattice constants along the z- (or x- or y-) axis also strongly develops in Regions III and IV, which reinforces the previous finding that antiferroelectriclike interactions exist within the BZT relaxor system. Note that the supplemental material [26] also provides and discusses the $\theta(\mathbf{r})$ function for all the $\mathbf{r}$-vectors lying in the (y, z) plane at 10 K.

A particularly important feature of our scheme is that we can switch on and off some interactions in order to determine their effect on physical properties. We numerically found that turning off random fields and random strains does *not* significantly affect the results shown in Fig. 1 and 2, which contrasts with a common belief on the microscopic origins of relaxors [4,16,17] while being more consistent

with models proposed for the homovalent (K, Li)TaO$_3$ relaxor [52,53]. On the other hand, our computations reveal that it is the difference in ferroelectric strength between Ti and Zr ions that leads to the relaxor behavior in BZT. As a matter of fact, annihilating such differences in the simulations leads to (1) χ^{direct} and χ^{CF} being equal to each other and continuously decreasing as the temperature decreases down to 0 K (with the system remaining cubic and nonpolar), (2) the Edwards-Anderson parameter being around 10 times smaller than the one depicted in Fig. 1(b) at low temperature, and (3) the polar nanoclusters disappearing. It should also be emphasized that our simulation results depicted in Figs. 1 and 2 imply that relaxor behavior can occur in BZT even if no large chemically ordered region exists in that system (since our computations were performed on disordered solid solutions). Such a finding seems to contrast with models recently proposed to explain the relaxor behavior of heterovalent Pb(Sc, Nb)O$_3$ and Pb(Mg, Nb)O$_3$ alloys [13], while agreeing with a study [39] downplaying the role of chemical short-range ordering on the formation of polar nanoregions in BZT. In fact, our simulations indicate that the relaxor behavior already occurs in *disordered* BZT solid solutions because some regions of space can be more Ti rich than others because of the random process of assigning sites in a disordered solid solution. Such a feature bears resemblance to the Anderson localization phenomenon for which electronic wave functions become localized in a region of space [of an overall disordered (A', A'') solid solution] that is much richer in A' than in A'' [54]. Finally, we also increased the antiferroelectriclike interactions (by playing with the so-called j_5 short-range coefficient [27]). We found that such an increase leads to a shift towards higher temperatures of the peak of χ^{CF}, in addition to enhancing at low temperatures (i) the Edwards-Anderson parameter, (ii) the average magnitude of the local modes centered on Ti ions, (iii) the square of the Fourier transform of the local dipoles configuration at $\mathbf{k}_{\max}$, and (iv) the strength of the anticorrelation between Ti dipoles that are distant by three lattice constants along the z- (or x- or y-) axis. Such findings emphasize the importance of the antiferroelectriclike interactions between Ti-rich nanopolar clusters for the relaxor behavior.

We therefore hope that our study helps in achieving a better understanding of the fascinating relaxor ferroelectrics. In order to further enhance such understanding, future studies could examine the influence of static and dynamic (GHz–THz) electric fields [20,21] on the behaviors of BZT materials, and determine if the results found here also hold for heterovalent relaxors [such as Pb(Sc, Nb)O$_3$ and Pb(Mg, Nb)O$_3$].

[1] L. E. Cross, Ferroelectrics **151**, 305 (1994).

[2] G. Burns and F. H. Dacol, Phys. Rev. B **28**, 2527 (1983).

[3] G. A. Smolensky *et al.*, *Ferroelectrics and Related Materials* (Gordon and Breach, New York, 1981).

[4] V. Westphal, W. Kleemann, and M. D. Glinchuk, Phys. Rev. Lett. **68**, 847 (1992).

[5] A. K. Tagantsev and A. E. Glazounov, Phys. Rev. B **57**, 18 (1998).

[6] R. Pirc and R. Blinc, Phys. Rev. B **60**, 13470 (1999).

[7] I.-K. Jeong, T. W. Darling, J. K. Lee, Th. Proffen, and R. H. Heffner, Phys. Rev. Lett. **94**, 147602 (2005).

[8] Y. Bai and L. Jin, J. Phys. D **41**, 152008 (2008).

[9] H. Vogel, Phys. Z. **22**, 645 (1921).

[10] G. S. Fulcher, J. Am. Ceram. Soc. **8**, 339 (1925).

[11] B. Dkhil, P. Gemeiner, A. Al-Barakaty, L. Bellaiche, E. Dul'kin, E. Mojaev, and M. Roth, Phys. Rev. B **80**, 064103 (2009).

[12] O. Svitelskiy, D. Orauttapong, J. Toulouse, W. Chen, and Z. G. Ye, Phys. Rev. B **72**, 172106 (2005).

[13] S. Tinte, B. P. Burton, E. Cockayne, and U. V. Waghmare, Phys. Rev. Lett. **97**, 137601 (2006).

[14] V. M. Ishchuk, V. N. Baumer, and V. L. Sobolev, J. Phys. Condens. Matter **17**, L177 (2005).

[15] N. Takesue, Y. Fujii, M. Ichihara, and H. Chen, Phys. Rev. Lett. **82**, 3709 (1999).

[16] R. Blinc, A. Gregorovič, B. Zalar, R. Pirc, V. V. Laguta, and M. D. Glinchuk, Phys. Rev. B **63**, 024104 (2000).

[17] B. E. Vugmeister and M. D. Glinchuk, Rev. Mod. Phys. **62**, 993 (1990).

[18] D. Viehland, S. J. Jang, L. E. Cross, and M. Wuttig, J. Appl. Phys. **68**, 2916 (1990).

[19] E. V. Colla, E. Y. Koroleva, N. M. Okuneva, and S. B. Vakhrushev, Phys. Rev. Lett. **74**, 1681 (1995).

[20] I. Grinberg, P. Juhas, P. K. Davies, and A. M. Rappe, Phys. Rev. Lett. **99**, 267603 (2007).

[21] A. Al-Zein, J. Hlinka, J. Rouquette, and B. Hehlen, Phys. Rev. Lett. **105**, 017601 (2010).

[22] C. Kittel, *Introduction to Solid State Physics* (Wiley, New York, 2004).

[23] Z. Kutnjak, C. Filipič, R. Pirc, A. Levstik, R. Farhi, and M. El Marssi, Phys. Rev. B **59**, 294 (1999).

[24] A. Levstik, Z. Kutnjak, C. Filipic, and R. Pirc, Phys. Rev. B **57**, 11204 (1998).

[25] S. F. Edwards and P. W. Anderson, J. Phys. F **5**, 965 (1975).

[26] See Supplemental Material at http://link.aps.org/supplemental/10.1103/PhysRevLett.108.257601 for more details about the effective Hamiltonian used here and correlation function.

[27] W. Zhong, D. Vanderbilt, and K. M. Rabe, Phys. Rev. B **52**, 6301 (1995).

[28] L. Bellaiche and D. Vanderbilt, Phys. Rev. B **61**, 7877 (2000).

[29] J. Iniguez and L. Bellaiche, Phys. Rev. B **73**, 144109 (2006).

[30] L. Bellaiche, A. García, and D. Vanderbilt, Phys. Rev. Lett. **84**, 5427 (2000); Ferroelectrics **266**, 41 (2002).

[31] S. Prosandeev and L. Bellaiche, Phys. Rev. Lett. **97**, 167601 (2006).

[32] P. Hohenberg and W. Kohn, Phys. Rev. **136**, B864 (1964).

[33] D. Vanderbilt, Phys. Rev. B **41**, 7892 (1990).

[34] I. A. Kornev, L. Bellaiche, P.-E. Janolin, B. Dkhil, and E. Suard, Phys. Rev. Lett. **97**, 157601 (2006).

[35] L. Walizer, S. Lisenkov, and L. Bellaiche, Phys. Rev. B **73**, 144105 (2006).

[36] Q. Zhang and I. Ponomareva, Phys. Rev. Lett. **105**, 147602 (2010).

[37] I. Ponomareva, L. Bellaiche, T. Ostapchuk, J. Hlinka, and J. Petzelt, Phys. Rev. B **77**, 012102 (2008).

[38] J. Hlinka, T. Ostapchuk, D. Nuzhnyy, J. Petzelt, P. Kuzel, C. Kadlec, P. Vanek, I. Ponomareva, and L. Bellaiche, Phys. Rev. Lett. **101**, 167402 (2008).

[39] R. L. L. Withers and B. Nguyen, Appl. Phys. Lett. **91**, 152907 (2007).

[40] T. Maiti, R. Gu, and A. S. Bhalla, J. Am. Ceram. Soc. **91**, 1769 (2008).

[41] A. García and D. Vanderbilt, in *First-Principles Calculations For Ferroelectrics: Fifth Williamsburg Workshop*, edited by R. E. Cohen (AIP, Woodbury, New York, 1998), p. 53.

[42] K. M. Rabe and E. Cokayne, in *First-Principles Calculations for Ferroelectrics: Fifth Williamsburg Workshop*, edited by R. E. Cohen (AIP, Woodbury, New York, 1998), p. 61.

[43] R. Fahri, M. E Marssi, A. Simon, and J. A. Ravez, Eur. Phys. J. B **9**, 599 (1999).

[44] J. Mydosh, *Spin Glasses: An Experimental Introduction* (Taylor and Francis, London-Washington, DC, 1993), pp. 139–143.

[45] A. Simon, J. Ravez, and M. Maglione, J. Phys. Condens. Matter **16**, 963 (2004).

[46] C. Laulhé, A. Pasturel, F. Hippert, and J. Kreisel, Phys. Rev. B **82**, 132102 (2010).

[47] Note that, in order to determine the actual atomic displacements of Ti and Zr atoms from our MC simulations, one has to multiply the results of Fig. 1(c) by the product of the lattice constant with the eigenvector of the force-constant matrix associated with Zr or Ti atoms. This product is of the order of 2.55 Å.

[48] A. Dixit, S. B. Majumder, R. S. Katiyar, and A. S. Bhalla, J. Mater. Sci. **41**, 87 (2006).

[49] A. M. George, J. Iñiguez, and L. Bellaiche, Phys. Rev. B **65**, 180301 (R) (2002).

[50] S. Mori, N. Yamamoto, Y. Koyama, and Y. Uesu, Phys. Rev. B **52**, 6158 (1995).

[51] A. R. Akbarzadeh, L. Bellaiche, K. Leung, J. Íñiguez, and D. Vanderbilt, Phys. Rev. B **70**, 054103 (2004).

[52] J. Toulouse, B. E. Vugmeister, and R. Pattnaik, Phys. Rev. Lett. **73**, 3467 (1994).

[53] B. E. Vugmeister and P. Adhikari, Ferroelectrics **157**, 341 (1994).

[54] L. W. Wang, L. Bellaiche, S. H. Wei, and A. Zunger, Phys. Rev. Lett. **80**, 4725 (1998).